PAPER

Check for updates

Fabricating highly hydrophobic thermoplastic starch/polyvinyl alcohol composites *via* twin-screw extrusion using citric acid–chitosan co-plasticizers

Tzu-Chin Chang, [a] Shi-Quan Chang, [b] Siang-Jia Jiang, [b] Yi-Ling Lu [b] and Shu-Ling Huang [*abc]

As one of the most prevalent polymers in nature, starch has the advantages of biodegradability, non-toxicity and low cost. Typically, starch granules can be broken down by gelatinization and plasticization in the presence of water and plasticizers to obtain thermoplastic starch (TPS). In this work, TPS was prepared by optimizing the water content (50 wt%) for corn starch gelatinization. TPS/polyvinyl alcohol (TPS/PVA) composites were successfully fabricated *via* extrusion and injection molding, using citric acid (CA) and chitosan (Cs) co-plasticizers. Structural analysis with ATR-FT/IR confirmed that CA and Cs underwent esterification and *N*-acetylation reactions with TPS and PVA, forming a cross-linked structure. Incorporating CA and Cs improved TPS/PVA composite compatibility with inorganic fillers, enhancing surface smoothness and processing stability. However, ATR-FT/IR, viscometer, oscillating shear rheometer and DSC tests demonstrated that when CA addition exceeded 15 wt%, TPS underwent significant acid hydrolysis of glycosidic bonds, resulting in decreased viscosity and even the disappearance of crystallinity. The findings showed that when CA addition was 10 wt% (TC10), the mechanical properties of the TPS/PVA composite improved significantly; accordingly, its tensile strength, elastic modulus, flexural strength, and flexural modulus increased by approximately 200%, 660%, 290%, and 220%, respectively. Furthermore, TC10 exhibits remarkable hydrophobicity, with its contact angle increasing from 75° to 110°. CA–Cs co-plasticization addresses the migration problem of conventional low molecular weight plasticizers under high temperature, significantly enhancing blending uniformity, mechanical properties, and water resistance. TPS/PVA composites are expected to become an ideal choice for environmentally friendly products.

1. Introduction

Starch, a natural polymer derived from abundant natural resources, exhibits advantages of biodegradability, non-toxicity, and low cost.[1,2] However, native starch with a crystallinity of 20–45% possesses poor mechanical strength and water resistance, which limits its potential to replace disposable plastic products.[3,4] In addition, native starch's poor processing ability, owing to numerous hydrogen bonds between starch macromolecules, inhibits the movement of these molecules.[5,6] In general, starch granules can be disrupted in the presence of water and plasticizers *via* gelatinization and plasticization to obtain thermoplastic starch (TPS).[7–10] TPS possesses a metastable amorphous structure that can be processed plastically with other fillers or biopolymers, demonstrating its potential

for single-use biodegradable products.[11–15] However, the use of pure TPS remains limited in molding processes, because of, for example, its mechanical brittleness, which triggers plasticizer migration and results in fast aging.[16,17] Strategies like blending TPS with other biodegradable polymers, including polyvinyl alcohol (PVA),[18] polylactide (PLA), poly(butylene adipate terephthalate) (PBAT),[19,20] polybutylene succinate (PBS), and poly(-butylene succinate-*co*-adipate) (PBSA),[21] can be employed to address these limitations. In addition to being water-soluble, PVA is highly biocompatible, biodegradable, printable, oil-resistant, chemical-resistant, and non-toxic. Hence, it has been utilized in packaging materials, polarizing plates, water transfer films, and mold release applications.[18] However, PVA exhibits poor thermoplastic processing properties owing to its ultra-strong intra- and intermolecular hydrogen bonding interactions, which severely limit its practical application in melt processing.[22,23]

Furthermore, in humid environments, PVA-based films are exposed to mechanical strength loss, limiting their potential as plastic alternatives.[24,25] Plasticization is the most prevalent physical method for improving the melt extrusion processing of

[a] Ph.D. Program in Material and Chemical Engineering, National United University, Miaoli 36003, Taiwan. E-mail: simone@nuu.edu.tw; Tel: +886-37-382-209

[b] Department of Chemical Engineering, National University, Miaoli 36003, Taiwan

[c] Science/International Master's Program in Translation Medicine, National United University, Miaoli 36003, Taiwan
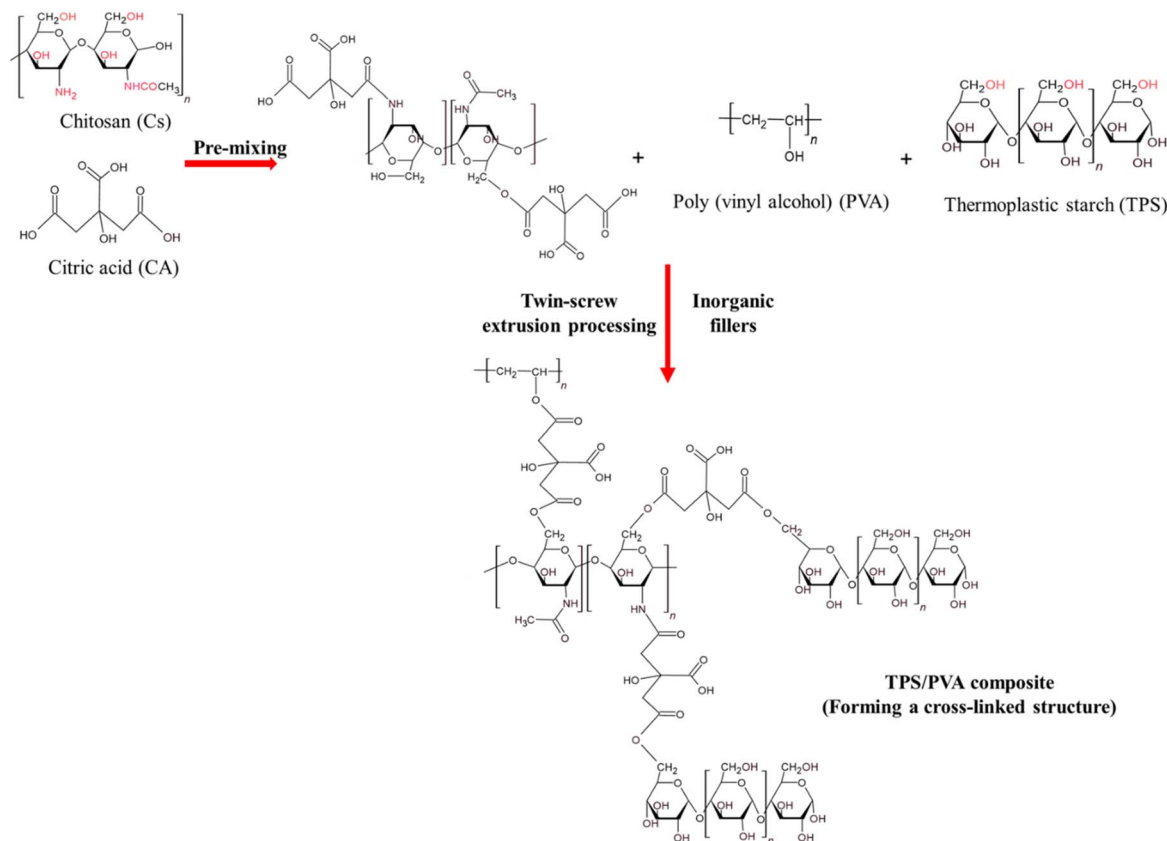
polymer materials.[26,27] The plasticizers employed include various small molecules containing several hydroxyl and amide groups,[28] such as water, glycerol, sorbitol, formamide,[29,30] and citric acid (CA).[31,32] These small-molecule compounds can destroy PVA or TPS internal interactions by forming new interactions, thus improving melt flow ability and achieving melt extrusion.[33,34] Recently, TPS/PVA blends have demonstrated positive synergies, in particular, significantly enhanced mechanical strength and toughness.[35,36] Nevertheless, they are limited by plasticizer migration due to starch retrogradation in long-term applications.[35] The development of citric acid–glycerol co-plasticized thermoplastic starch (CGTPS) was initially reported in 2007, representing the initial discovery of this co-plasticization approach.[3] The novel CGTPS exhibited special properties of partial esterification, low molecular weight, and stronger interaction between starch and plasticizers. The esterification (ED) and degree of substitution (DS) increased as the CA content increased, while the molecular weight decreased as the CA percentage increased for CGTPS. Partial esterification could influence the starch chains for potential modification, thus improving compatibility. These special properties render CGTPS a potential candidate in various field applications. Recently, several studies have explored using CA with glycerol to co-plasticize TPS/PVA, improving water solubility, migration, and mechanical properties. A novel 3D plasticizer based on an esterified citric acid–glycerol mixture, with a higher molecular weight than glycerol, was prepared as previously reported.[35] This co-plasticizer is based on a maximum esterified CA–glycerol mixture, achieving a slower migration process of low molecular weight plasticizers owing to the increase in steric limitations. A thermoplastic starch/citric acid (TPS/CA) blend was fabricated with excess CA as a plasticizer, yielding an approximately 20-fold reduction in the average molecular weight of the TPS.[37] This implies that the crosslinking of CA with starch hydrolysis was simultaneous as the blending process occurred under highly acidic conditions (pH ∼ 2). Although starch hydrolysis increases the plasticizing effect, it causes a significant decrease in mechanical strength. CA has been previously utilized as a compatibilizer in a thermoplastic starch/polylactic acid (TPS/PLA, 60 : 40 w/w) blend to enhance its thermal stability.[38] Starch-based straws containing CA, boric acid, talc, and stearic acid, and treated with hot oxalic acid, were developed to enhance material performance.[39] Starch-based straws can be smoothly processed, significantly reducing water absorption (55.3%) and improving mechanical properties (modulus) by approximately 54% compared to neat starch. The findings provided a beneficial guideline for developing starch-based materials with low moisture sensitivity. This study clarified how screw speed affects the mechanical strength and water resistance of starch straws during thermoplastic extrusion, providing a theoretical basis for the industrial production of starch straws.[40] Several morphological changes in the crystal regions of structures can be observed during starch gelatinization and plasticization.

Both PVA and starch are highly hydrophilic because of the numerous hydroxyl groups in their molecular chains. Recently, several studies have focused on improving the hydrophobicity of the TPS/PVA blend.[41–47] As reported previously,[48] hydrophobic starch-based nanofibers (HPS) with different HPS/PVA (HPA) mass ratios were fabricated via electrospinning to improve the hydrophobicity of the surface of composite films. A hydrophobic surface was formed on the HPA film via CA self-assembly coating, increasing the water contact angle from 30.95° to 100.74°. The hydrophobicity of starch/PVA composites was further enhanced by introducing a carbon-black inorganic filler and increasing the PVA content from 3 wt% to 5 wt%, increasing the contact angle from 78.0° to 85.0°.[49]

A review explores various factors ranging from structural properties to physicochemical and environmental conditions that may impact polymer biodegradability.[53] Chitosan (Cs) is a key multifunctional biopolymer in biodegradable polymer systems valued for its film-forming ability, biocompatibility, and intrinsic antimicrobial activity.[54] The structural integrity and durability of composite materials are determined by the molecular interactions between Cs and other biopolymers. Cs contains amino ($-NH_3^+$) and hydroxyl ($-OH$) groups that form hydrogen bonds and electrostatic interactions with polysaccharides such as starch or pectin, and with PVA, creating a cohesive polymer network with enhanced interfacial adhesion and structural strength. When blended with proteins or polysaccharides, its cationic nature at acidic pH enables the formation of polyelectrolyte complexes through electrostatic attraction with negatively charged residues, improving flexibility and mechanical robustness. Furthermore, the bioactivity of Cs can be enhanced via synergistic interactions with other polymers or natural extracts, effectively inhibiting microbial growth and degradation. These interactions are strongly influenced by the degree of deacetylation, molecular weight, and blend ratio, as well as processing parameters such as plasticizer or crosslinker content. Consequently, such interpolymer interactions are fundamental to improving the mechanical durability, hydrophobicity, and long-term stability of biodegradable starch-based composites for extrusion or injection-molding applications.[55] The literature[35] indicates that compared to a single glycerol-based system, citric acid–glycerol-derived oligomer co-plasticizers can reduce the migration of plasticizers and improve mechanical stability. This benchmark comparison highlights that the design of a CA–Cs co-plasticizer shows a relative advantage for preparing TPS/PVA composites, as CA–Cs co-plasticization can effectively inhibit plasticizer migration, while also providing chitosan-derived bioactivity.[53–55] Our previous research presented an optimized blending formula for TPS/PVA, where introducing an acidic chitosan (Cs) aqueous solution to replace the glycerol plasticizer can effectively inhibit glycerol migration during melt processing. However, although these formulas can effectively improve the plasticizer migration problem, they also inhibit the blend and inorganic filler's fluidity and uniformity, and fail to improve hydrophobicity. Therefore, we utilized a CA–Cs co-plasticizer that enhances the compatibility of TPS/PVA blends, in addition to producing a co-crosslinking synergistic effect with TPS and PVA via esterification (CA–starch, CA–PVA, or CA–Cs) and N-acetylation (CA–Cs) reactions. The co-plasticizer can also effectively block the numerous hydroxyl groups present in PVA and TPS,

Scheme 1 The proposed mechanism of the CA–Cs co-plasticized TPS/PVA composite production.

significantly increasing the hydrophobicity of TPS/PVA composites. Scheme 1 presents the proposed mechanisms of the CA–Cs co-plasticized TPS/PVA composite production.

2. Materials and methods

2.1 Materials

Corn starch was purchased from Tai Roun Products Co., Ltd (Taiwan). Chitosan (Cs) with a degree of deacetylation of 86.72% was purchased from Charming & Beauty Co., Ltd (Taiwan). Acetic acid (purity 99.7%) was purchased from ECHO Chemical Co., Ltd (Taiwan). Citric acid was purchased from TTCA Co., Ltd (China). PVA with a polymerization degree of 1700 and a hydrolysis degree of 99% was purchased from Chang Chun Petrochemical Co., Ltd (Taiwan). Calcium carbonate was purchased from the Far Eastern Co., Ltd (Taiwan). Silicon dioxide was purchased from Ruoya Ark International Trading Co., Ltd (Taiwan).

2.2 Fabrication of TPS/PVA blends

2.2.1 TPS preparation. Corn starch was introduced to different water content levels in a reaction vessel and stirred. The water ratio was 35 wt% to 60 wt% (w35–w60), and the initial TPS was obtained by gelatinizing at 80 °C for 2 h. Then, the chemical structure and thermal properties of the samples were analyzed at 25 °C using attenuated total reflectance Fourier-transform infrared spectroscopy (ATR-FT/IR) and a differential scanning calorimeter (DSC).

2.2.2 TPS/PVA premixing with CA–Cs co-plasticizers. Cs (5 g) was added to a 100 mL aqueous acid solution and stirred until gelatinous for later use. PVA (120 g) and 500 mL of water were placed into a pre-mixer, heated, and stirred at 160 °C for 30 min. Subsequently, 600 g of TPS (gelatinized corn starch in 50 wt% of water, w50) was added into the resulting mixture and stirred for 10 min at 80 °C. The TPS/PVA blends were added to a pre-mixed Cs solution with various CA amounts (0 wt%, 10 wt%, 15 wt%, and 20 wt%), and then heated and stirred at 80 °C for 15 min. A constant content of calcium carbonate and silica was introduced into the TPS/PVA blends and stirred evenly at 30 °C for 10 min. The resulting mixtures were labelled as TC0 (0 wt%), TC10 (10 wt%), TC15 (15 wt%), and TC20 (20 wt%).

2.2.3 TPS/PVA composite processing with co-plasticization using a twin-screw extruder. Subsequently, a twin-screw extruder ($L/D = 44$, $D = 20$ mm) (CHT20, Nan Yun Industrial Co., Ltd, Taiwan) was utilized to process the TPS/PVA composites. Five heating zones (85, 90, 95, 100, and 95 °C) were adopted from the feeding barrel to the die, and the speed values of the feeding barrel and extruder engine were set at 20 and 200 rpm, respectively. The pre-mixed TPS/PVA blending powders were fed from the feeding barrel, extruded through the die, and cut into the masterbatch. The TPS/PVA composite masterbatch can be utilized in injection molding to produce the standard test

pieces. Test specimens were accorded to ASTM D638 and D790 using an injection molding machine (SM-90, CHEN HSONG, Taiwan) with a temperature range of 120–140 °C, an injection speed of 30–60%, a maximum injection pressure of 320–720 bar, and a cooling time of 30 s.

2.3 Characteristic analysis

2.3.1 Functional group analysis by ATR-FT/IR. The functional group analysis of TPS and TPS/PVA with co-plasticizers was conducted using ATR-FT/IR (Thermo Nicolet™ iS™ 10, USA) in the range of 4000–600 cm^{-1}, at a 0.7 times per s scan rate.

2.3.2 Surface morphological observation. The interfaces and cross-section morphologies of the samples were observed *via* SEM (ZEISS ULTRA PLUS, Germany) at an acceleration voltage of 3 kV at ×3000 magnification. An atomic force microscope (AFM) (Dimension Icon XR, Bruker, USA) was employed to observe the surface morphology at 25 °C, and the tapping mode was selected. The surface roughness of different samples was also recorded.

2.3.3 Thermal property measurement. Thermal analysis of the sample was performed using DSC (Q10, TA Instruments, and USA). The composites were broken into fragments, weighed to 3–5 mg of the sample, and placed in a sample dish of aluminum. The heating and cooling rates were set at 10 °C min^{-1} between 40 °C to 250 °C.

2.3.4 Mechanical properties. The bending strength of the samples was measured using a universal tester (A1-7000-S, GoTech, Taiwan) according to ASTM D790 guidelines. The maximum bending force (F_b) was expressed as the maximum positive pressure. The tensile strength of the samples was evaluated in accordance with ASTM D638. The crosshead runs at a speed of 20 mm min^{-1}. All results provided used the average of at least three specimens.

2.3.5 Measurement of migration degree and hydrophilicity/hydrophobicity. Circular specimens (7 mm diameter, 1 mm thickness) were prepared. These specimens were placed between two iron plates with absorbent paper tissues above and below. They were subjected to mild pressure (16.5 kPa) and kept in an oven at 60 °C for 7 days. The mass of the migrated plasticizer was determined in triplicate, by weighing specimens at different times (1–7 days) and calculating the weight loss with respect to the initial weight, as expressed in eqn (1).[35]

$$\text{Migration degree } (\%) = \left(\frac{m_0 - m_f}{m_0} \right) \times 100 \qquad (1)$$

where m_0 and m_f are the initial and final masses, respectively.

To evaluate the hydrophilic/hydrophobic properties, the contact angle between water and the samples was directly measured using a contact angle instrument (FTA-125, APPR, Germany). Deionized water (3 μL) was dropped onto the surface of the specimen by injection molding. Each measurement was conducted on five independent specimens, and the data are reported as the mean ± SD (standard deviation), with $n = 5$.

2.3.6 Measurement of viscosity and oscillatory shear rheology. The sample was ground, passed through a 100-mesh screen, and dried at 85 °C for 30 min. A 5 g sample was soaked and stirred with 195 g of water for 20 min at 90 °C, and then placed into an aluminum tube of a viscometer (MODEL DV-III Programmable Rheometer, Brookfield, USA) with a rotor number of SC4-27D-100 to test the viscosity at a 200 rpm rotating speed. Rheological assessment was conducted on a rotational rheometer (Kinexus Pro+, Malvern, UK; Netzsch, Germany) utilizing a 20 mm stainless steel parallel geometry at a gap height of 0.8 mm. The storage G' and loss G'' modulus as functions of the frequency ω were determined. Measurements were performed with a constant strain of 0.5%.[56,57]

3. Results and discussion

3.1 Corn starch gelatinization

3.1.1 Structural analysis. Water plays a crucial role in the gelatinization and physical plasticization of native starch. As the medium for starch endothermic transformation, it transforms from a solid or semi-crystalline state to a thermoplastic state with thermo-plasticity and ductility. The ratio of starch to water directly influences the gelatinization rate, degree of granule expansion, amount of amylose released, and viscosity/structure of the final paste. Corn starch possesses intramolecular hydrogen bonds that curl into a helical structure. After gelatinization or plasticization by water molecules, the hydrogen bond structures are altered. The intramolecular and intermolecular hydrogen bonds can be distinguished based on the wavenumber change, bandwidth, and intensity characteristics of the IR absorption band relative to the interaction.[10] From Fig. 1, all samples exhibit hydroxyl stretching vibration absorption peaks (ν-OH) in the range of 3600–3200 cm^{-1}, corresponding to the hydrogen bonds formed in the samples. The pure corn starch sample demonstrates that it primarily consists of intramolecular hydrogen bonds. Under thermal gelatinization, as the amount of water increases, water molecules enter the gaps between starch crystallites, thereby destroying the intramolecular hydrogen bonds between linear and branched structures and forming intermolecular hydrogen bonds with water molecules; consequently, the width and intensity of the absorption peak increase significantly. As the amount of water
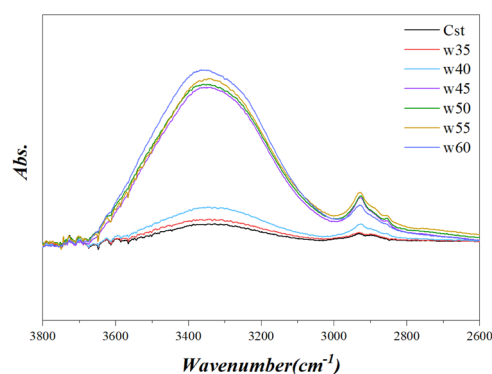

Fig. 1 Structural analysis of corn starch samples gelatinized with different water contents by ATR-FT/IR spectroscopy in the range of 3600–2600 cm^{-1}.

increases to 45–55 wt% (w45, w50, and w55), similar wavenumber regions, absorption peak intensities, and width effects emerge, implying that the intermolecular hydrogen bonds between water molecules and starch reached saturation. Under higher water content conditions (w60), a water solvent dilution effect is present, resulting in a wider and higher absorption peak intensity.

3.1.2 **Thermal property analysis.** Research in the literature shows[50] that waxy starch has 100 wt% amylopectin structures, exhibiting a single endothermic peak enthalpy value in thermal analysis with DSC. This is unlike corn starch, with an amylose/amylopectin ratio of approximately 28/72, for which thermal analysis shows multiple endothermic enthalpy values. This is because the number of endothermic enthalpy peaks depends on the amylose/amylopectin ratio; in addition, factors like water content, lipid content, and measurement conditions are closely related to the native starch's gelatinization effect. Starch with a high amylopectin proportion will produce a higher endothermic enthalpy value, and the total gelatinization enthalpy value increases with the increase in amylopectin and water content, but not linearly. For starch gelatinization with a higher water content, the main contribution to the total enthalpy stems from the water solvent assisting the disintegration of the amylopectin structure. DSC thermal property analysis shows that increasing water content leads to evident changes in both the crystallization melting temperature (T_m) and gelatinization enthalpy change (ΔH_m) of the TPS samples (Table 1). It can be deduced that, in an anhydrous environment, the un-gelatinized sample is mainly stabilized by intramolecular hydrogen bonds within starch molecules. In addition, the crystal structure is dense; hence, it exhibits the highest crystallization melting temperature (T_m) of approximately 183 °C, and the crystallization melting enthalpy is 25.8 J g^{-1}, which is primarily attributed to the endothermic enthalpy of melting the corn starch crystal region.

As the amount of water increases under thermal gelatinization, water molecules enter the gaps between starch microcrystals, resulting in irreversible large amounts of water absorption. In addition, the crystal region partially disintegrates, significantly reducing T_m. However, the gelatinization enthalpy increases with the water content due to the water solvent effect. When the amount of water increases to 50 wt% (w50), T_m decreases to the lowest point (140 °C), which implies that the maximum saturated water absorption state is achieved

between the starch microcrystals and water molecules. When the amount of water continued to increase to 55 wt% and 60 wt% (w55 and w60), the excess water shrank the gelatinized starch and separated it from the water at a lower temperature. The intramolecular hydrogen bonds between the linear and amylopectin structures slowly formed, which led to regular crystallization again, called retrogradation or the aging phenomenon. Hence, T_m increased to 150 °C. Based on the ATR-FT/IR results, functional group structure and thermal properties, it can be deduced that the best gelatinization effect is achieved when the water amount is 50 wt% (w50) under 80 °C thermal gelatinization.

3.2 Analyses of structure and viscosity/rheological properties of TPS/PVA composites with co-plasticizers

3.2.1 **Structural analyses.** The esterification and *N*-acetyl reactions of TPS/PVA composites with CA and Cs co-plasticizers can be verified *via* ATR-FT/IR in three ranges of 3300–2500 cm^{-1} (OH), 1163 cm^{-1} and 1149 cm^{-1} (C–O), and 1744 cm^{-1} and 1698 cm^{-1} (C=O), and involved the disappearance of carboxylic acid groups for CA.

Subsequently, it can be determined that the characteristic peaks of ester and amide groups were more significant because CA with TPS or Cs triggered the esterification and *N*-acetyl reactions, leading to peaks at 1720 cm^{-1} (C=O, in ester), 1300 cm^{-1} (C–O, in ester), and at 1630 cm^{-1}, 1580 cm^{-1}, and 1540 cm^{-1} (C=O, C–N, and N–H in amide).[32,51]

Fig. 2(a) and (b) illustrate that the heights of these peaks increased with the CA percentage. In particular, the characteristic absorption peak of CA (1390 cm^{-1}, δ_{CH}) appeared in the T10–T20 samples, which proved that the CA–Cs co-plasticization produced a cross-linked structure for TPS/PVA, as shown in Fig. 2(b). In addition, the characteristic peak of the glycosidic bond (C–O–C) was weakened as the CA content increased at 875 cm^{-1} and 1025 cm^{-1}. When the CA addition amount was 20 wt%, the peak disappeared at 875 cm^{-1}, as illustrated in Fig. 2(c). It can be speculated that a higher CA content may induce higher acid hydrolysis of the glycosidic linkages for starch.

3.2.2 **Viscosity alterations.** The IR results implied that when the amount of CA exceeded 15 wt%, the characteristic peak of the glycosidic bond gradually disappeared. It can be inferred that the higher the CA content, the greater the acid hydrolysis of the glycosidic bond.

Viscosity measurement (shown in Fig. 3) can also confirm that after adding 10 wt% CA, owing to the co-plasticization triggered by esterification and *N*-acetyl reactions, including the crosslinking effect, the viscosity of TC10 increased slightly. When the CA was added to 15 wt%, the viscosity decreased significantly, and the trend in the results agreed with the literature.[52]

3.2.3 **Rheological properties.** Oscillatory shear rheology was utilized to examine the viscoelastic behavior of the CA-modified TPS/PVA composites. Fig. 4 presents the dynamic frequency sweeps at 0.5% strain for samples with different CA contents. Within the angular frequency range of 0.1–10 rad s^{-1},

Table 1 Thermal analysis of gelatinized corn starch samples with different water contents

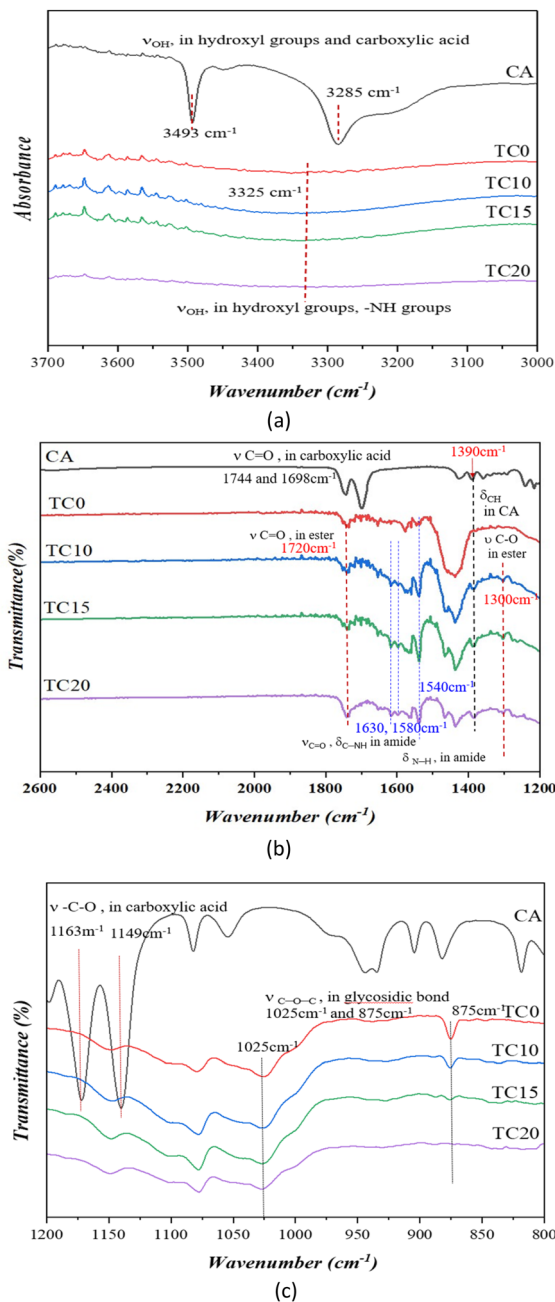| Sample	T_m (°C)	ΔH_m (J g^{-1})
Corn starch	183	25.8
w35	172	41.4
w40	168	49.6
w45	156	60.7
w50	140	97.5
w55	150	94.9
w60	150	99.5

(a)

(b)

(c)

Fig. 2 ATR-FT/IR spectra of (a) the 3700–3000 cm^{-1} region, (b) the 2600–1200 cm^{-1} region, and (c) the 1200–800 cm^{-1} region.

the average storage modulus (G') values were approximately 23, 29, 17, and 11 kPa for TC0, TC10, TC15, and TC20, respectively. The higher G' observed in TC10 indicates enhanced intermolecular interactions and partial crosslinking induced by esterification and N-acetyl reactions between CA/Cs and the hydroxyl groups of starch/PVA. This increase in G' suggests that CA functions as a plasticizer and a crosslinking agent, improving the elasticity and structural integrity of the composite. In contrast, further increasing the CA concentration (TC15 and TC20) resulted in a pronounced decrease in G', implying that excess CA addition may cause over-plasticization and partial
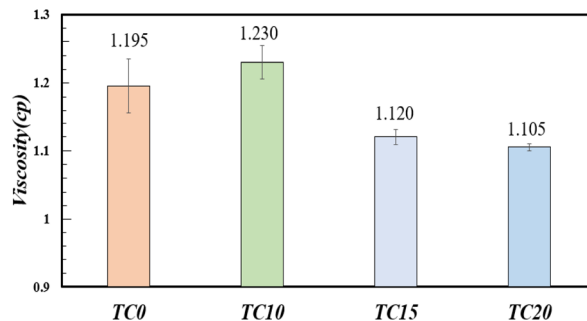

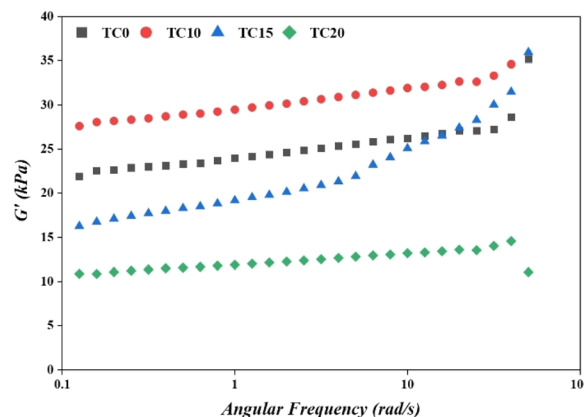**Fig. 3** Viscosity alterations for various samples.

Fig. 4 Dynamic frequency sweeps at 0.5% strain for TPS/PVA with different CA contents.

hydrolysis of glycosidic linkages, weakening the network structure. These rheological results confirm a co-plasticization–crosslinking balance that governs the processability and overall performance of the composites.[56,57]

3.2.4 Surface morphology observation. To further observe the effect of inorganic fillers and CA–Cs co-plasticization on the phase separation of the surface morphology, with the inorganic filler content kept at a maximized 30 wt%, surface morphology observation was performed by SEM and AFM analyses. Fig. 5 presents SEM images of the surface morphology of samples containing different proportions of CA at a constant Cs content. From Fig. 5(a), it can be observed that TC0 without adding CA exhibits evident holes or cracks on the surface. In the TC10 with 10 wt% CA added, the co-plasticization effect between CA and Cs enhanced the density and smoothness, as illustrated in Fig. 5(b). From the IR spectra and viscosity alteration results, it is evident that when the CA content increased to over 15 wt%, the excess CA resulted in the acid hydrolysis reaction of starch. The inorganic fillers resulted in partial phase separation and surface smoothness loss, as illustrated in Fig. 5(c) and (d).

In addition, the influence of CA-induced crosslinking on the nanoscale surface topography was examined by AFM.[58–60] As illustrated in Fig. 6(a)–(c), the TC0 sample had a highly irregular surface with pronounced height fluctuations, resulting in a large roughness average (RA) of 83.3 ± 32.3 nm and a broad
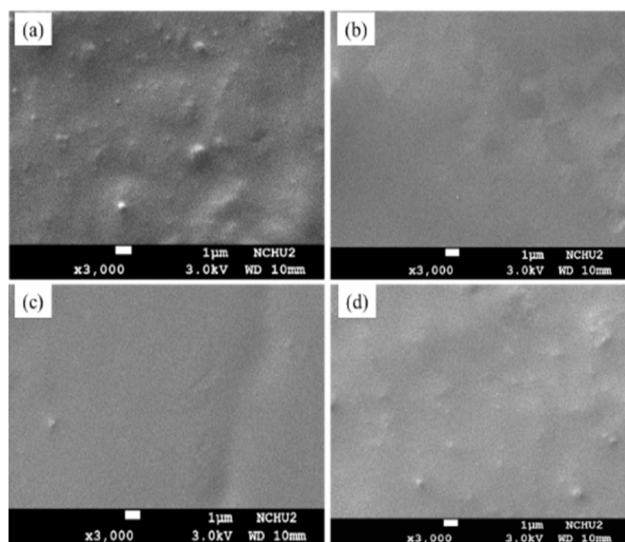
Fig. 5 SEM images of the samples with different proportions of CA with constant Cs: (a) TC0, (b) TC10, (c) TC15, and (d) TC20.

height distribution. In contrast, the TC10 sample had a remarkably smoother and more uniform surface, with RA reduced to 2.2 ± 0.9 nm, and a much narrower distribution. For TC15 and TC20, the roughness increased again (RA = 22.0 ± 6.4 nm and 26.8 ± 9.8 nm, respectively), reflecting a partial loss of surface uniformity at higher CA contents. As illustrated in Fig. 6(c), the statistical roughness distribution clearly narrows upon incorporation of an optimal amount of CA (TC10), demonstrating that CA/Cs co-plasticization effectively smoothens the composite surface by enhancing molecular cohesion within the polymer network.

3.3 Thermal properties of TPS/PVA composites with co-plasticizers

The exothermic and endothermic peaks can be observed from Fig. 7, which correspond to the samples' T_m and T_c. The enthalpies of crystalline melting (ΔH_m) and crystallization (ΔH_c) can be calculated using the integrated area, as summarized in Table 2. The results showed that the TC0 sample exhibits higher T_m and T_c compared with the CA-containing composites. At a CA content of 10 wt% (TC10), T_m and T_c decreased slightly; however, at 15 wt% of CA, T_c decreased from 97 °C to 86 °C. When the CA content reached 20 wt% (TC20), T_m and T_c disappeared, implying that the glycosidic linkages of starch were broken at higher CA content, such that the crystal structures also collapsed.

3.4 Appearance of specimens and mechanical properties by injection molding

3.4.1 Appearance of specimens by injection molding. Analysis using IR spectroscopy, viscosity, thermal properties, SEM, and AFM revealed that the TC10 sample exhibited optimal formability and surface smoothness. Fig. 8 presents the appearance of TC10 with extrusion/injection molding for
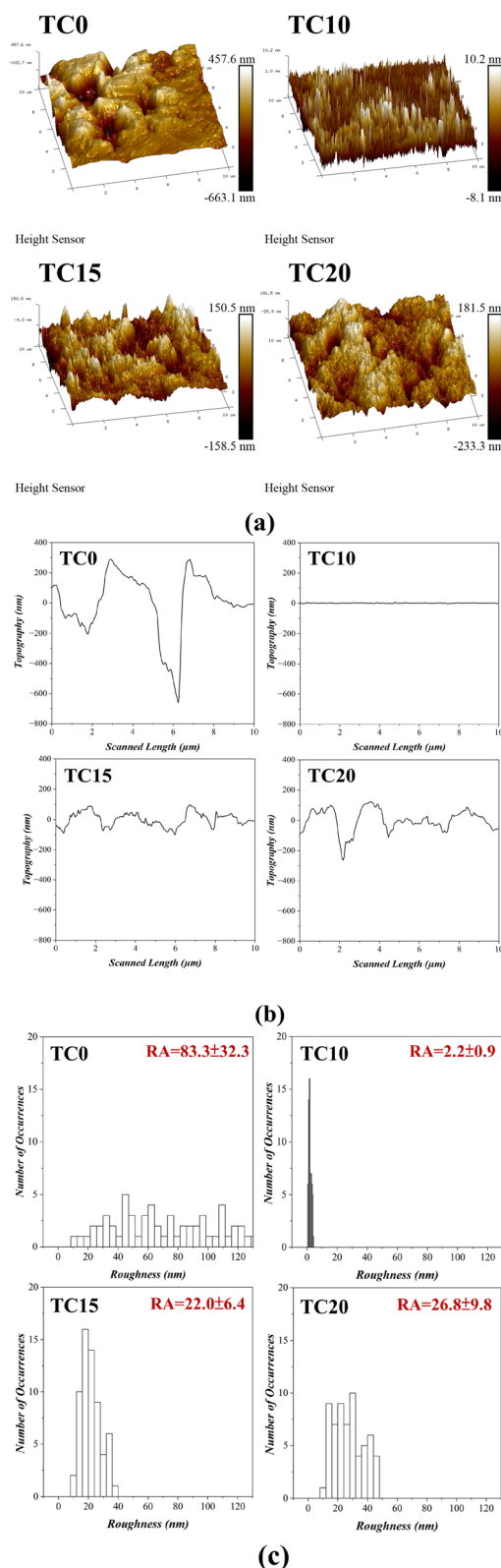

Fig. 6 (a) AFM topography images of a 10.0 × 10.0 μm surface section, (b) corresponding surface height profiles, and (c) roughness distributions of sample surfaces.
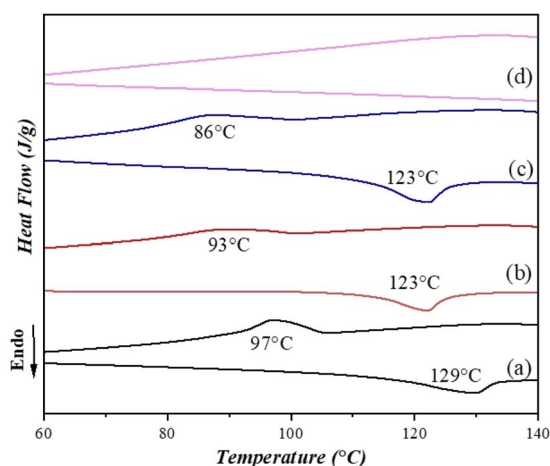
Fig. 7 DSC heat flow curves through the cycle of heating–cooling for TPS/PVA with different CA contents: (a) TC0, (b) TC10, (c) TC15, and (d) TC20.

Table 2 Thermal properties of samples with different proportions of CA at constant Cs

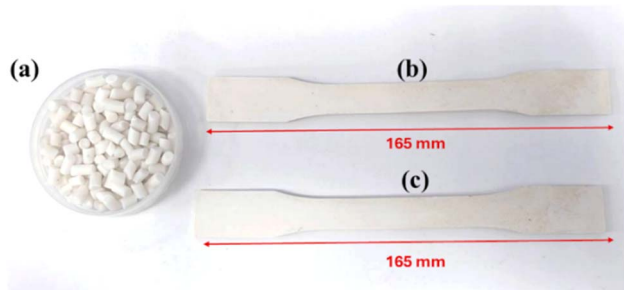| Sample	T_m (°C)	T_c (°C)	ΔH_m (J g^{-1})	ΔH_c (J g^{-1})
TC0	129	97	5.73	5.60
TC10	123	93	4.15	2.80
TC15	123	86	4.56	3.35
TC20	N.D.	N.D.	N.D.	N.D.

Fig. 8 Appearance of (a) TC10 pellets, (b) a TC10 dumbbell specimen, and (c) a TC10-6M specimen after 6 months of storage.

qualitative durability and aging evaluation. The pellets and dumbbell specimens of TC10 are illustrated in Fig. 8(a) and (b), respectively. The TC10-6M dumbbell-shaped specimen showed no significant changes in size, color, cracks, or surface morphology after six months of environmental storage, as illustrated in Fig. 8(c). It retained its macroscopic integrity, indicating that the CA–Cs co-plasticized TPS/PVA composites possess a certain level of long-term stability.

3.4.2 Tensile test. From IR spectra and viscosity analysis, we determined that the glycosidic bond of starch (TC20) triggered the acidification and hydrolysis owing to a high CA content, thus decreasing the molecular weight. Therefore, the TC20 sample cannot be modelled through injection processing
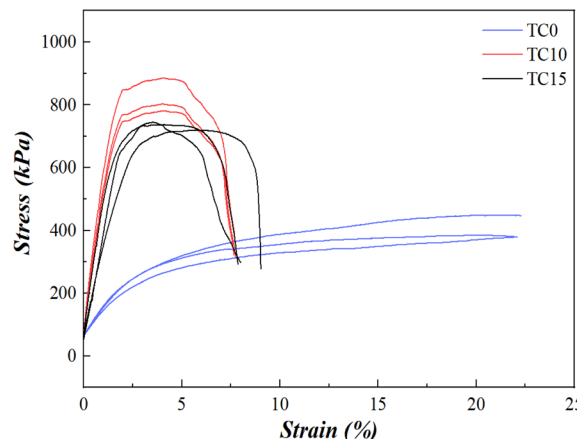

Fig. 9 Stress–strain curves of TPS/PVA with different CA contents.

Table 3 Mechanical properties of TPS/PVA with different CA contents

Sample	Tensile strength (kPa, avg.)	Elongation at break (%, avg.)	Elastic modulus (MPa, avg.)
TC0	387.3	22.1	8.9
TC10	784.1	7.3	58.6
TC15	722.4	8.3	49.9

and the measured mechanical properties. Fig. 9 presents the stress–strain curves for TPS/PVA with different CA contents with triple repeat; in addition, the tensile strength, elongation at break, and elastic modulus are presented in Table 3. From the results above, it can be deduced that the 10 wt% CA–Cs co-plasticized TPS/PVA composite (TC10) exhibits the best mechanical properties. Notably, the elastic modulus increased from 8.9 MPa to 58.6 MPa, of which more than 650% was achieved without addition (TC0).

3.4.3 Three-point flexural test. The analysis of three-point flexural mechanical properties exhibited similar results to the tensile test. To compare with the TC0 sample, the addition of an appropriate amount of CA–Cs co-plasticized TPS/PVA composite with a cross-linked network structure was carried out. The flexural strength and flexural modulus of TC10 were significantly enhanced by about 290%. In addition, a sample (TC10-6M) after six months of ambient storage was evaluated for aging, and it was found that the attenuation of the flexural strength and flexural modulus was below 3%, indicating that the CA/Cs co-plasticized TPS/PVA composites demonstrated good anti-aging in mechanical strength, as illustrated in Fig. 10 and Table 4.

3.5 Migration analyses and hydrophilic/hydrophobic properties

3.5.1 Migration degree. As presented in Table 5, the migration degree did not increase after the third day, and the migration degree of all samples was below 0.5%. Compared with conventional single plasticizers (*e.g.* glycerol) with a migration degree above 10%,[35,61] the migration degree of the
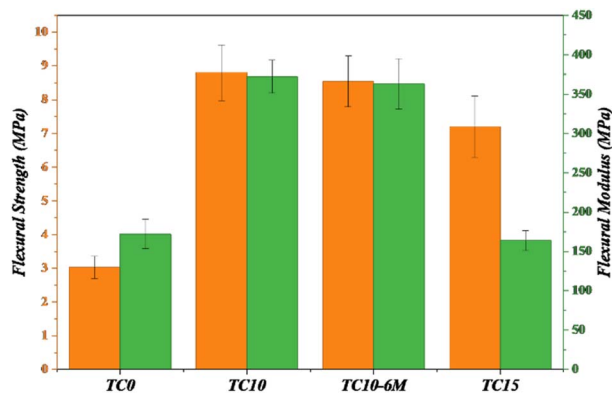
Fig. 10 Comparison charts of flexural strength (orange) and flexural modulus (green) for TPS/PVA with different CA contents and anti-aging evaluation.

Table 4 Flexural strength and flexural modulus for various TPS/PVA composites

Sample	Flexural strength (MPa, avg.)	Flexural modulus (MPa, avg.)
TC0	3.03	172.10
TC10	8.80	372.00
TC10-6M[a]	8.54	362.72
TC15	7.20	164.00

[a] Specimen was stored under ambient laboratory conditions for six months.

Table 5 Migration degree of TPS/PVA composites with different CA contents

Migration degree (%)	TC0	TC10	TC15
Day 1	0.04	0.00	0.27
Day 2	0.13	0.11	0.26
Day 3	0.32	0.11	0.44
Day 5	0.32	0.11	0.44
Day 7	0.32	0.11	0.44

TC10 sample was only about 0.11%, which is almost negligible. The results confirm that the optimal CA/Cs ratio (TC10) further improves the migration problem of conventional plasticizers, confirming that the co-plasticized network structure effectively suppresses small-molecule release.

3.5.2 Contact angle analyses. The contact angle can be utilized to determine the hydrophilic/hydrophobic properties of a substance's surface. Highly hydrophilic materials exhibit smaller contact angles, while highly hydrophobic materials exhibit larger contact angles, typically greater than 90°. Fig. 11 shows that TC10 is highly hydrophobic and that its contact angle is as high as $110 \pm 2.33°$, which is attributed to the co-plasticization effect of CA/Cs. However, a higher CA content induced greater acid hydrolysis of the glycosidic linkages, also resulting in a decreased contact angle ($83.88 \pm 1.88°$), as seen in
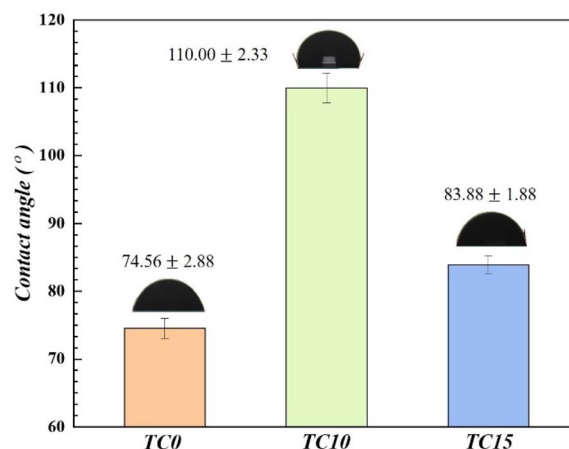

Fig. 11 Contact angles of TPS/PVA with different CA contents.

the TC15 sample. Improved surface hydrophobicity is essential for enhancing the surface stability and cleanliness of molded biodegradable materials. A more hydrophobic surface resists water adhesion and moisture penetration, thus maintaining a smooth, contamination-free surface morphology. This phenomenon is consistent with previous findings,[54,61] which reported that higher surface hydrophobicity promotes water repellency and anti-fouling behavior, improving surface durability of polymeric materials. The intrinsic biodegradability of a polymer is determined by the chemical structure and resulting physical properties. Polymers with higher molecular weight, higher crosslinking, lower water solubility, and a higher degree of substitution may result in reduced biodegradability. In general, carbon-chain polyolefins are not biodegradable. However, according to quantitative structure–activity relationship (QSAR) studies reported in the literature,[62] polymers containing unstable bonds such as ester bonds, ether bonds, amide bonds, or glycosidic bonds might be more biodegradable. Although CA-induced crosslinking is expected to reduce water solubility and disintegration (compared to pure TPS), TPS/PVA composites with ester or amide bonds formed through CA–Cs co-plasticization can still hydrolyze under composting or moist soil conditions.

4. Conclusions

TPS/PVA composites were modified *via* co-plasticization with CA and Cs. The findings indicated that the best comprehensive performance was obtained when 10 wt% CA (TC10) was added. Structural analysis verified that CA and Cs produced the esterification/*N*-acetyl co-plasticization effect, forming a cross-linked structure, increasing the compatibility between starch, PVA, and inorganic fillers, as well as improving surface smoothness and process stability. However, adding 20 wt% of CA triggered severe acid hydrolysis of the TPS/PVA composite, resulting in the cleavage of glycosidic bonds on the starch matrix. Therefore, with the appropriate CA content (10 wt%), the TPS/PVA composite's mechanical properties were significantly improved, demonstrating excellent toughness and rigidity. In addition,

TC10 exhibited remarkable hydrophobicity with a contact angle of approximately 110°. In addition to solving the migration problem of conventional plasticizers, CA–Cs co-plasticization results in optimal mechanical properties, water resistance, antimicrobial characteristics, and processing stability. Therefore, utilizing a co-plasticizer of citric acid and chitosan is appropriate for injection-molded TPS/PVA articles, considering both processability and performance. These obtained composites have potential applications in single-use biodegradable rigid products, such as pet toys, children's toys, chopsticks, cutlery, screws, plant pots, and decorative items, which will ultimately address the environmental pollution crisis.

Author contributions

Conceptualization and supervision: Tzu-Chin Chang and Shu-Ling Huang; methodology and investigation: Tzu-Chin Chang, Shi-Quan Chang and Shu-Ling Huang; resources: Tzu-Chin Chang and Shu-Ling Huang; literature review and writing—original draft preparation: Tzu-Chin Chang, Shi-Quan Chang and Shu-Ling Huang; data curation: Tzu-Chin Chang, Siang-Jia Jiang and Yi-Ling Lu; writing—review and editing: Tzu-Chin Chang and Shu-Ling Huang. All authors have read and agreed to the published version of the manuscript.

Conflicts of interest

The authors declare that they have no conflicts of interest.

Data availability

The datasets generated and analyzed in this current study are available from the corresponding author upon reasonable request.

Acknowledgements

References

1 H.-Y. Kim, J.-l. Jane and B. Lamsal, *Ind. Crops Prod.*, 2017, **95**, 175–183.

2 D. Rahardiyan, E. M. Moko, J. S. Tan and C. K. Lee, *Enzyme Microb. Technol.*, 2023, **168**, 110260.

3 R. Shi, Z. Zhang, Q. Liu, Y. Han, L. Zhang, D. Chen and W. Tian, *Carbohydr. Polym.*, 2007, **69**, 748–755.

4 H. F. Zobel, *Starch/Staerke*, 1988, **40**, 44–50.

5 E. Ojogbo, E. O. Ogunsona and T. H. Mekonnen, *Mater. Today Sustain.*, 2020, **7–8**, 100028.

6 Y. Yang, J. Fu, Q. Duan, H. Xie, X. Dong and L. Yu, *Foods*, 2024, **13**, 4036.

7 K. E. Rivadeneira-Velasco, C. A. Utreras-Silva, A. Díaz-Barrios, A. E. Sommer-Márquez, J. P. Tafur and R. M. Michell, *Polymers*, 2021, **13**, 3227.

8 T. Jiang, Q. Duan, J. Zhu, H. Liu and L. Yu, *Adv. Ind. Eng. Polym. Res.*, 2020, **3**, 8–18.

9 A. Surendren, A. K. Mohanty, Q. Liu and M. Misra, *Green Chem.*, 2022, **24**, 8606–8636.

10 D. Donmez, L. Pinho, B. Patel, P. Desam and O. H. Campanella, *Curr. Opin. Food Sci.*, 2021, **39**, 103–109.

11 H. Cheng, L. Chen, D. J. McClements, T. Yang, Z. Zhang, F. Ren, M. Miao, Y. Tian and Z. Jin, *Trends Food Sci. Technol.*, 2021, **114**, 70–82.

12 S. Jayarathna, M. Andersson and R. Andersson, *Polymers*, 2022, **14**, 4557.

13 P. F. Muñoz-Gimena, V. Oliver-Cuenca, L. Peponi and D. López, *Polymers*, 2023, **15**, 2972.

14 S. X. Tan, A. Andriyana, H. C. Ong, S. Lim, Y. L. Pang and G. C. Ngoh, *Polymers*, 2022, **14**, 664.

15 F. Xie, P. Liu and L. Yu, in *Starch Polymers*, ed. P. J. Halley and L. Avérous, Elsevier, Amsterdam, 2014, pp. 257–289.

16 N. Khanoonkon, K. M. Dang and R. Yoksan, *Int. J. Biol. Macromol.*, 2024, **280**, 136335.

17 H. Tian, J. Yan, A. V. Rajulu, A. Xiang and X. Luo, *Int. J. Biol. Macromol.*, 2017, **96**, 518–523.

18 J. Zhou, Y. Ma, L. Ren, J. Tong, Z. Liu and L. Xie, *Carbohydr. Polym.*, 2009, **76**, 632–638.

19 J. Hong, J. Lee, S. K. Kim, D. Son, D. Kang and J. K. Shim, *Polymers*, 2025, **17**, 138.

20 C. Zhang, Z. Sun, X. Yang, G. Duan, M. Wang and Y. Qiao, *BioResources*, 2025, **20**, 3910–3922.

21 C. Martín-Poyo, J. P. Cerisuelo-Ferriols and J. D. Badia-Valiente, *Appl. Sci.*, 2025, **15**, 456.

22 Z. W. Abdullah, Y. Dong, I. J. Davies and S. Barbhuiya, *Polym.-Plast. Technol. Eng.*, 2017, **56**, 1307–1344.

23 N. Chen, L. Li and Q. Wang, *Plast., Rubber Compos.*, 2007, **36**, 283–290.

24 V. T. Nguyen, L. H. Pham, N. T. Nguyen and D. Hoang, *Int. J. Biol. Macromol.*, 2025, **318**, 144988.

25 J. Xu, L. Ren, W. Song, N. Wu and R. Zeng, *Ind. Crops Prod.*, 2024, **209**, 117975.

26 T. Mekonnen, P. Mussone, H. Khalil and D. Bressler, *J. Mater. Chem. A*, 2013, **1**, 13379–13398.

27 Z. Eslami, S. Elkoun, M. Robert and K. Adjallé, *Molecules*, 2023, **28**, 6637.

28 M. I. J. Ibrahim, S. M. Sapuan, E. S. Zainudin and M. Y. M. Zuhri, *Int. J. Food Prop.*, 2019, **22**, 925–941.

29 A. Baran, P. Vrábel, M. Kovaľaková, M. Hutníková, O. Fričová and D. Olčák, *J. Appl. Polym. Sci.*, 2020, **137**, 48964.

30 J. Yan, H. Tian, Y. Zhang and A. Xiang, *J. Appl. Polym. Sci.*, 2015, **132**, 42364.

31 W. Zhang, S. Roy, E. Assadpour, X. Cong and S. M. Jafari, *Adv. Colloid Interface Sci.*, 2023, **314**, 102886.

32 K. Wilpiszewska, A. K. Antosik and M. Zdanowicz, *J. Polym. Environ.*, 2019, **27**, 1379–1387.

33 K. Junlapong, P. Boonsuk, C. Chaibundit and S. Chantarak, *Int. J. Biol. Macromol.*, 2019, **137**, 521–527.

34 R. Jumaidin, S. N. Mohd Zainel and S. M. Sapuan, in *Advanced Processing, Properties, and Applications of Starch and Other Bio-Based Polymers*, ed. F. M. Al-Oqla and S. M. Sapuan, Elsevier, 2020, pp. 11–19.

35 J. M. Castro, M. G. Montalbán, N. Martínez-Pérez, D. Domene-López, J. M. Pérez, F. M. Arrabal-Campos, I. Fernández, I. Martín-Gullón and J. C. García-Quesada, *Int. J. Biol. Macromol.*, 2023, **244**, 125478.

36 F. Kahvand and M. Fasihi, *Int. J. Biol. Macromol.*, 2019, **140**, 775–781.

37 C. Menzel, E. Olsson, T. S. Plivelic, R. Andersson, C. Johansson, R. Kuktaite, L. Järnström and K. Koch, *Carbohydr. Polym.*, 2013, **96**, 270–276.

38 K. Martínez-Villadiego, M. J. Arias-Tapia and A. F. Jaramillo, *Polym. Bull.*, 2024, **81**, 13253–13274.

39 M. Yang, F. Jun, M. Alee, Q. Duan, H. Xie, A. Ali, H. Liu, L. Chen and L. Yu, *J. Appl. Polym. Sci.*, 2023, **140**, 4036.

40 K. Wang, C. Tan, H. Tao, F. Yuan, L. Guo and B. Cui, *Carbohydr. Polym.*, 2024, **328**, 121701.

41 X. Tang and S. Alavi, *Carbohydr. Polym.*, 2011, **85**, 7–16.

42 C. Chen, L. Zong, J. Wang and J. Xie, *Carbohydr. Polym.*, 2021, **272**, 118448.

43 X. Wei, H. Tao, C. Tan, J. Xie, F. Yuan, L. Guo, B. Cui, F. Zou, W. Gao, P. Liu and L. Lu, *Int. J. Biol. Macromol.*, 2023, **239**, 124211.

44 Y. Yao, Y.-I. Hsu and H. Uyama, *Ind. Crops Prod.*, 2024, **222**, 119870.

45 P. K. Panda, K. Sadeghi and J. Seo, *Food Packag. Shelf Life*, 2022, **33**, 100904.

46 M. Cheng, R. Kong, R. Zhang, X. Wang, J. Wang and M. Chen, *Ind. Crops Prod.*, 2021, **171**, 113864.

47 Z. Wu, Y. Huang, L. Xiao, D. Lin, Y. Yang, H. Wang, Y. Yang, D. Wu, H. Chen, Q. Zhang, W. Qin and S. Pu, *Int. J. Biol. Macromol.*, 2019, **123**, 569–575.

48 W. Pan, Q. Liang and Q. Gao, *Int. J. Biol. Macromol.*, 2022, **223**, 1297–1307.

49 G. Irmukhametova, K. M. Al Azzam, G. A. Mun, L. Bekbayeva, Z. Dinara, B. B. Yermukhambetova, S. V. Nechipurenko, S. A. Efremov, E.-S. Negim and M. Samy, *Polymers*, 2025, **17**, 479.

50 H. Liu, L. Yu, F. Xie and L. Chen, *Carbohydr. Polym.*, 2006, **65**, 357–363.

51 F. Cheng, B. Wang and Y. Xia, *Int. J. Polym. Sci.*, 2018, **2018**, 4960416.

52 W. C. Chen, S. N. M. Syed Mohd Judah, S. K. Ghazali, D. I. Munthoub, H. Alias, Z. Mohamad and R. Abd Majid, *Italian Association of Chemical Engineering*, 2021, **83**, 199–204.

53 D. H. U. Eranda, M. Chaijan, I. Uysal-Unalan, W. Panpipat, A. S. Naik, A. L. Dib, S. Karnjanapratum and M. Gagaoua, *Food Biosci.*, 2024, **58**, 103696.

54 D. H. Udana Eranda, M. Chaijan and R. Castro-Muñoz, *J. Food Eng.*, 2025, **391**, 112440.

55 D. H. U. Eranda, M. Chaijan, W. Panpipat, S. Karnjanapratum, M. A. Cerqueira and R. Castro-Muñoz, *Int. J. Biol. Macromol.*, 2024, **280**, 135661.

56 M. Kim, K. L. D. M. Weerawardene, W. Choi, S. M. Han, J. Paik, Y. Kim, M.-G. Choi, C. M. Aikens and D. Lee, *Chem. Mater.*, 2020, **32**, 10216–10226.

57 S. Sarkar, C. F. Anderson and J. P. Schneider, *Angew. Chem., Int. Ed.*, 2024, **63**, e202313507.

58 K. Dey, S. R. Chowdhury, E. Dykstra, A. Koronatov, H. P. Lu, R. Shinar, J. Shinar and P. Anzenbacher, *J. Mater. Chem. C*, 2020, **8**, 11988–11996.

59 K. Dey, S. Roy Chowdhury, E. Dykstra, H. P. Lu, R. Shinar, J. Shinar and P. Anzenbacher Jr, *ACS Appl. Electron. Mater.*, 2021, **3**, 3365–3371.

60 A. Zhong, R. Tao, R. Zong, S. Liu and B. Shentu, *RSC Adv.*, 2025, **15**, 7248–7256.

61 N. Khanoonkon, K. M. Dang and R. Yoksan, *Int. J. Biol. Macromol.*, 2024, **280**, 136335.

62 J. R. Kim, J.-R. Thelusmond, V. C. Albright III and Y. Chai, *Sci. Total Environ.*, 2023, **890**, 164338.